

Article

Application of MnO₂ Nanorod–Ionic Liquid Modified Carbon Paste Electrode for the Voltammetric Determination of Sulfanilamide

Hadi Beitollahi¹, Somayeh Tajik^{2,*} and Antonio Di Bartolomeo^{3,*} 

¹ Environment Department, Institute of Science and High Technology and Environmental Sciences, Graduate University of Advanced Technology, Kerman 7631885356, Iran; h.beitollahi@kgut.ac.ir

² Research Center of Tropical and Infectious Diseases, Kerman University of Medical Sciences, Kerman 7616913555, Iran

³ Physics Department “E.R. Caianiello”, University of Salerno, Via Giovanni Paolo II 132, 84084 Fisciano, Italy

* Correspondence: s.tajik@kmu.ac.ir (S.T.); adibartolomeo@unisa.it (A.D.B.)

Abstract: The current work introduced a convenient single-phase hydrothermal protocol to fabricate MnO₂ nanorods (MnO₂ NRs). Fourier transform infrared spectroscopy (FT-IR), X-ray diffraction (XRD), Energy-dispersive X-ray spectroscopy (EDX) and field-emission scanning electron microscopy (FE-SEM) were used to determine the characteristics of MnO₂ NR. Then, ionic liquid (IL) and MnO₂ NRs were utilized to modify a carbon paste electrode (CPE) surface (MnO₂NR-IL/CPE) to voltammetrically sense the sulfanilamide (SAA). An enhanced voltammetric sensitivity was found for the as-developed modified electrode toward SAA when compared with a bare electrode. The optimization experiments were designed to achieve the best analytical behavior of the SAA sensor. Differential pulse voltammetry (DPV) in the optimized circumstances portrayed a linear dependence on various SAA levels (between 0.07 and 100.0 μM), possessing a narrow detection limit (0.01 μM). The ability of the modified electrode to be used in sensor applications was verified in the determination of SAA present in the actual urine and water specimens, with impressive recovery outcomes.

Keywords: MnO₂ nanorod; ionic liquid; sulfanilamide; electrochemical sensor; voltammetry



Citation: Beitollahi, H.; Tajik, S.; Di Bartolomeo, A. Application of MnO₂ Nanorod–Ionic Liquid Modified Carbon Paste Electrode for the Voltammetric Determination of Sulfanilamide. *Micromachines* **2022**, *13*, 598. <https://doi.org/10.3390/mi13040598>

Academic Editor: Josue Ortiz-Medina

Received: 7 March 2022

Accepted: 8 April 2022

Published: 10 April 2022

Publisher’s Note: MDPI stays neutral with regard to jurisdictional claims in published maps and institutional affiliations.



Copyright: © 2022 by the authors. Licensee MDPI, Basel, Switzerland. This article is an open access article distributed under the terms and conditions of the Creative Commons Attribution (CC BY) license (<https://creativecommons.org/licenses/by/4.0/>).

1. Introduction

Sulfonamides (SAs) are agents that were able to show a selective effect on bacteria for the first time. They are systematically prescribed to control bacterial infections. The structure of sulfonamides contains an amino group bound with a phenyl ring having an alkyl sulfonamide in the para direction [1,2]. 4-aminobenzenesulfonamide, also called sulfanilamide or SAA, with the formula C₆H₈N₂O₂S is an antibiotic with antibacterial activity. The antibacterial response of SAA is related to the competitive inhibition of dihydropterase synthetase relative to paminobenzoate [3,4]. Despite the numerous benefits of antibiotics, they are potential contaminants. Hence, there are numerous reports of adverse effects on human health and the formation of resistant bacteria following long-term and over-administration of antibiotics. The biotic and abiotic degradability of SAA is weak in nature, so its residues can be found in various aquatic solutions like waste treatment plant effluents, surface water and groundwater, which is a public health problem worldwide [5,6]. This introduction highlights the need to take a robust approach to quantifying SAA at trace levels in different environments.

There are multiple accurate techniques for sensing the SAA, some of which are liquid chromatography [7], high performance liquid chromatography [8,9], spectrophotometry [10], chemiluminescence [11], and capillary electrophoresis-mass spectrometry [12]. However, some of these methods have disadvantages such as a high cost, a time-consuming operation, unsuitability for on-site analysis, and the need for qualified operators and complicated instrumentations.

Among all sensing systems, great attention has been focused on the electrochemical determinations owing to their impressive merits like simple use, affordability, portability, exceptional selectivity, and sensitivity and rapidity [13–19]. Voltammetry has had a great role in the detection of various analytes in environmental, biomedical and food matrices. Numerous studies reported the direct detection of analytes by voltammetry owing to accuracy, convenience, simplicity, sensitivity, and rapidity [20–23]. Hence, the SAA concentrations can also be detected by voltammetric methods. A major problem in this field is the need for a high overpotential due to the direct redox reaction of analytes on the bare electrode, as a result of which the appeared fouling impact leads to a weakness in reproducibility and selectivity [24,25].

Electrode surface modification can increase the sensitivity of the produced sensors due to the establishment of appropriate and adjustable features. Diverse modifiers in this field have offered a lower limit of detection (LOD), excellent sensitivity, overpotential reduction and surface fouling resistance [26–32].

The use of appropriate electrochemical methods in conjunction with carbon paste electrodes (CPEs) has yielded acceptable results. A variety of analytes have been detected by CPEs because of their unique properties, some of which include residual currents 10 times lower than glassy carbon electrodes (GCEs), a wider potential window, and facile preparation steps [33–38]. The selectivity and sensitivity of the target analyte determination can be significantly enhanced by chemically modified CPEs using modifiers [39–42].

One of the most successful modifiers used in electrochemical sensors is nanoparticles (NPs), and many special features of the working electrode, like the huge surface area and small size, reproducibility, peak current and sensitivity, can be enhanced in the presence of NPs [43,44].

Another modifiers are metal oxides, owing to their admirable traits, some of which include an adjustable production, huge specific surface area, direct paths for electron transfer, empty space to reduce volume expansion, proper adhesion of active substance to current collector and low cost [45,46]. A popular oxide material is manganese dioxide (MnO_2), whose behavior can be enhanced by changing its morphology and surface area. MnO_2 is a polymorph (1D α -, β - and γ - MnO_2 , and 2D δ - MnO_2) owing to an octahedral $[\text{MnO}_6]$ spatial arrangement [47,48]. Nano-sized MnO_2 exhibits commendable benefits, due to a larger surface-to-volume ratio and further reactive surface for electrochemical reactions. The diverse application of this substance in electrochemistry and sensor fabrication can be attributed to the simple reduction of MnO_2 to Mn_2O_3 and MnO and, at the proper potential, the re-oxidation to MnO_2 as a catalytic circle for electrochemical detection [49–51].

Electroanalysis and electrochemistry have recently benefited greatly from room temperature ionic liquids (RTILs), which have astonishing physicochemical properties such as an impressive thermal and chemical stability, ionic architecture, proper extraction capacity, low equilibrium vapor pressure, ion exchange activity, potent conductivity and broad electrochemical window. ILs have a better conductivity than paraffin oil, which makes them suitable for making paste electrodes in voltammetric determinations due to a reduced charge current and consequent intensification of sensitivity and a decrease in the LOD value [52,53].

Accordingly, the present study utilized these two compounds to modify the CPE surface.

The current work introduced a convenient single-phase hydrothermal protocol to fabricate MnO_2 NR. Then, IL and MnO_2 NR were utilized to modify the CPE surface to voltammetrically sense the SAA. An enhanced voltammetric sensitivity was found for the as-developed modified electrode toward SAA when compared with the bare CPE. The ability of the modified electrode for use in sensor applications was verified in the determination of SAA present in the real specimens, with an impressive relative standard deviation (RSD).

2. Materials and Methods

2.1. Chemicals and Equipment

An X-ray diffractometer (Panalytical X'Pert Pro, Almelo, The Netherlands) using copper/ $K\alpha$ radiation ($\lambda = 1.5418 \text{ \AA}$) captured XRD patterns. A Tensor II spectrometer (Bruker, Denzendorf, Baden-Württemberg, Germany) was utilized to record the FT-IR spectra. A scanning electron microscope (MIRA3, Tescan, Brno, Czech Republic) provided the FE-SEM images and the EDX patterns. An autolab potentiostat/galvanostat (PGSTAT-302N, Eco Chemie, Utrecht, The Netherlands) recorded all electrochemical determinations. The General Purpose Electrochemical System (GPES) as selected software monitored all testing protocols. A conventional three-electrode system was used at $25 \pm 1 \text{ }^\circ\text{C}$. An Ag/AgCl/KCl (3.0 M) electrode, a platinum wire and $\text{MnO}_2\text{NR-IL/CPE}$ were used as the reference, auxiliary and working electrodes, respectively. A pH meter (Metrohm type 713) was utilized to determine all solution pH values. All solutions were prepared freshly by deionized water (DIW, Millipore Direct-Q[®] 8 UV water purification system, Darmstadt, Germany). Sulfanilamide, 1-butyl-3-methylimidazolium hexafluorophosphate (BMIM- PF_6) ionic liquid, and all materials were purchased from Merck (Darmstadt, Germany) with analytical research purity. Orthophosphoric acid as well as relevant salts have been applied to achieve all phosphate buffer solutions (PBS), set in a pH range of 2.0–9.0.

2.2. Hydrothermal Synthesis of MnO_2 NRs

The MnO_2 NRs were obtained by dissolving KMnO_4 (0.316 g) in deionized water (30 mL) while vigorously stirring, followed by the addition of 3 M HCl (1.4 mL) under vigorous stirring for another half hour. Then, the solution was placed in a 50-mL Teflon-lined autoclave at $160 \text{ }^\circ\text{C}$ for six hours. Next, the products were cooled down to room temperature and subsequently centrifuged and thoroughly rinsed with ethanol and deionized water to clean any impurity, followed by drying at $60 \text{ }^\circ\text{C}$ for 12 h.

2.3. Process of Electrode Fabrication

As the composition of the carbon paste is very important in electrochemical responses, we optimized all of them. To produce an MnO_2 NR and ionic liquid-modified carbon paste electrode ($\text{MnO}_2\text{NR-IL/CPE}$), firstly, ionic liquid (0.8 mL), MnO_2 NR (0.4 g), and graphite powder (0.9 g) were blended well together in a mortar to achieve a uniformly wetted paste. Then, the paste was compressed into the bottom of a glass tube. A copper wire was embedded into the back of the mixture down in a glass tube to establish an electrical contact. Next, excess paste, if present, was expelled from the tube, and a weighing paper was used for polishing to achieve a new surface.

3. Results and Discussion

3.1. Determination of Characteristics

Figure 1 illustrates the FE-SEM images captured for the as-fabricated MnO_2 NRs, and observing them confirmed rod-shaped MnO_2 nanostructures with a thickness ranging from 15 to 25 nm and a length of about 3 μm . The MnO_2 NRs showed an almost uniform size distribution.

The EDS analysis was performed to check the elemental composition of the MnO_2 NRs. Figure 2 shows the presence of O (42.16 wt%) and Mn (57.84 wt%) in the structure of MnO_2 NRs without any impurity.

Figure 3 displays the FT-IR spectrum captured for as-fabricated MnO_2 NRs, with the characteristic peaks at 476, 532 and 729 cm^{-1} corresponding to Mn-O α -phase vibration. The FT-IR spectrum of the as-prepared sample was consistent with the previous report [54].

Figure 4 portrays the XRD spectrum captured for MnO_2 NRs, presenting a clear crystallinity at sharp intense peaks. There were peaks with corresponding planes at 12.7 (110), 18 (200), 28.7 (310), 36.5 (400), 37.6 (121), 42 (301), 49.8 (411), 56.1 (521), 60.2 (002), 65.5 (451) and 69.6° . The diffraction peaks of MnO_2 related to a tetragonal architecture with the α phase, with ref. code 01-072-1982.

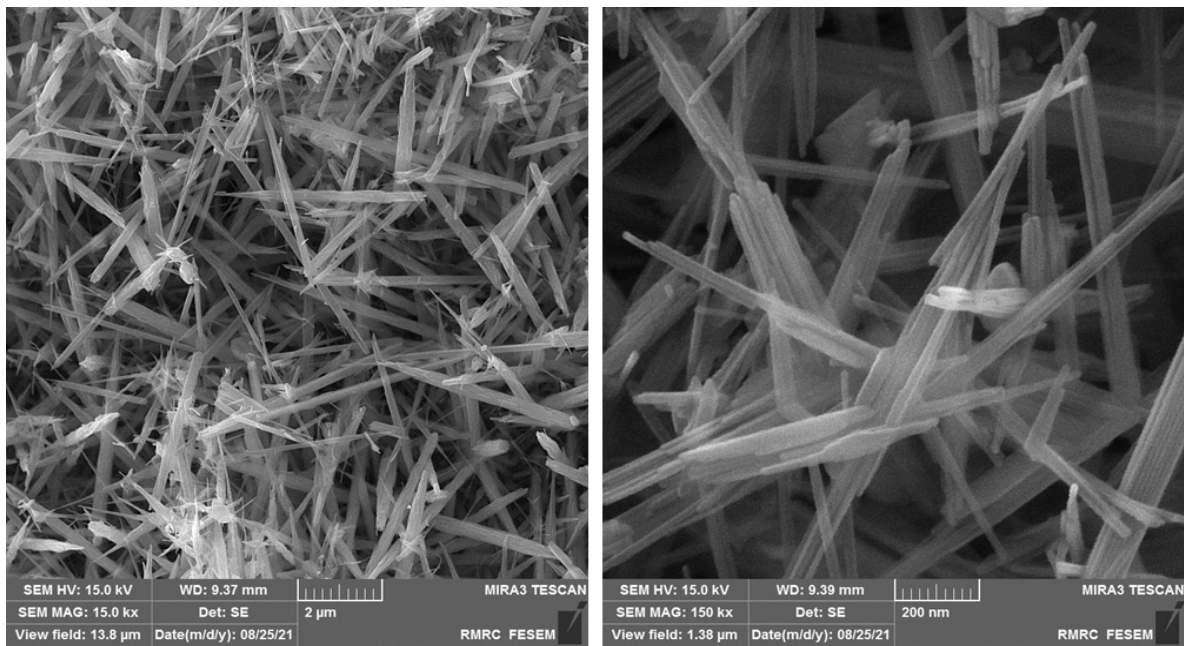


Figure 1. FE-SEM images captured for as-fabricated manganese dioxide nanorods, with various magnifications.

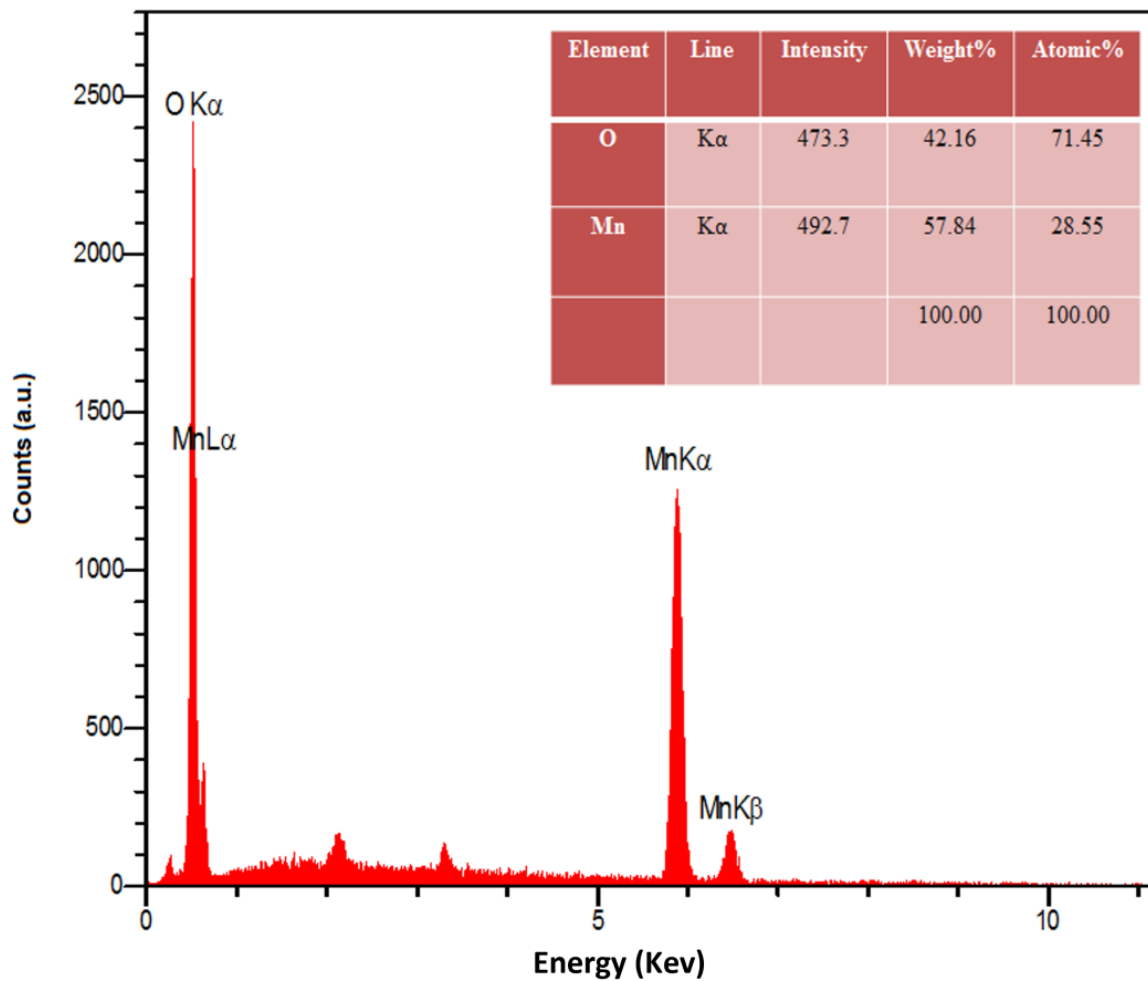


Figure 2. EDX spectrum captured for as-fabricated manganese dioxide nanorods.

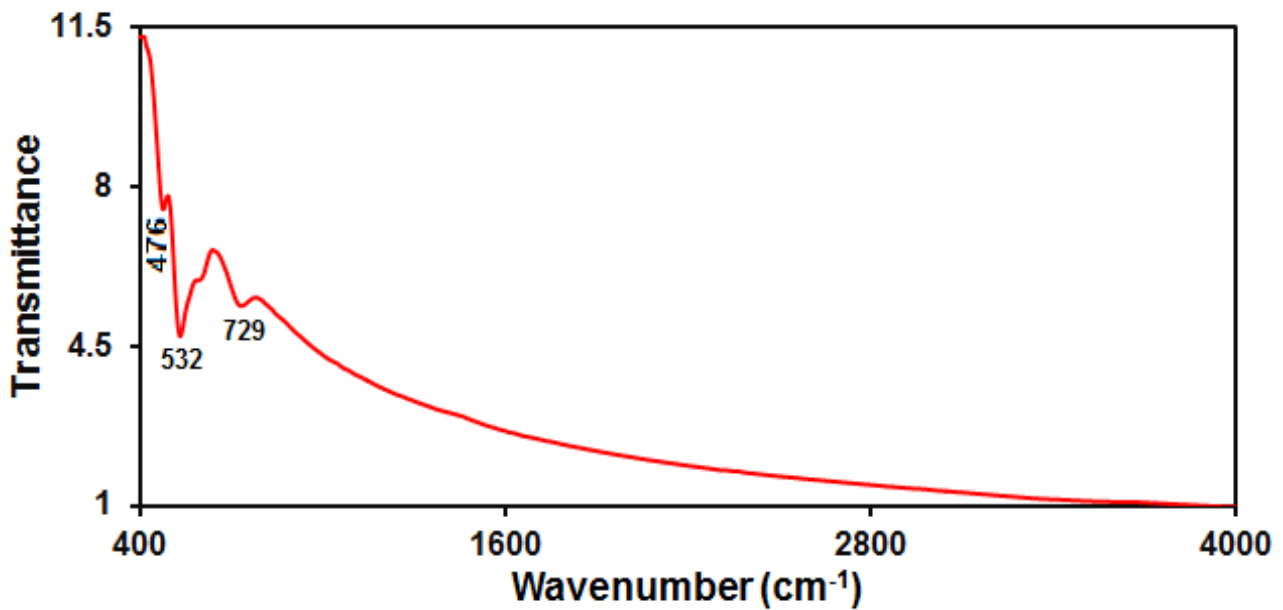


Figure 3. FT-IR pattern captured for as-fabricated manganese dioxide nanorods.

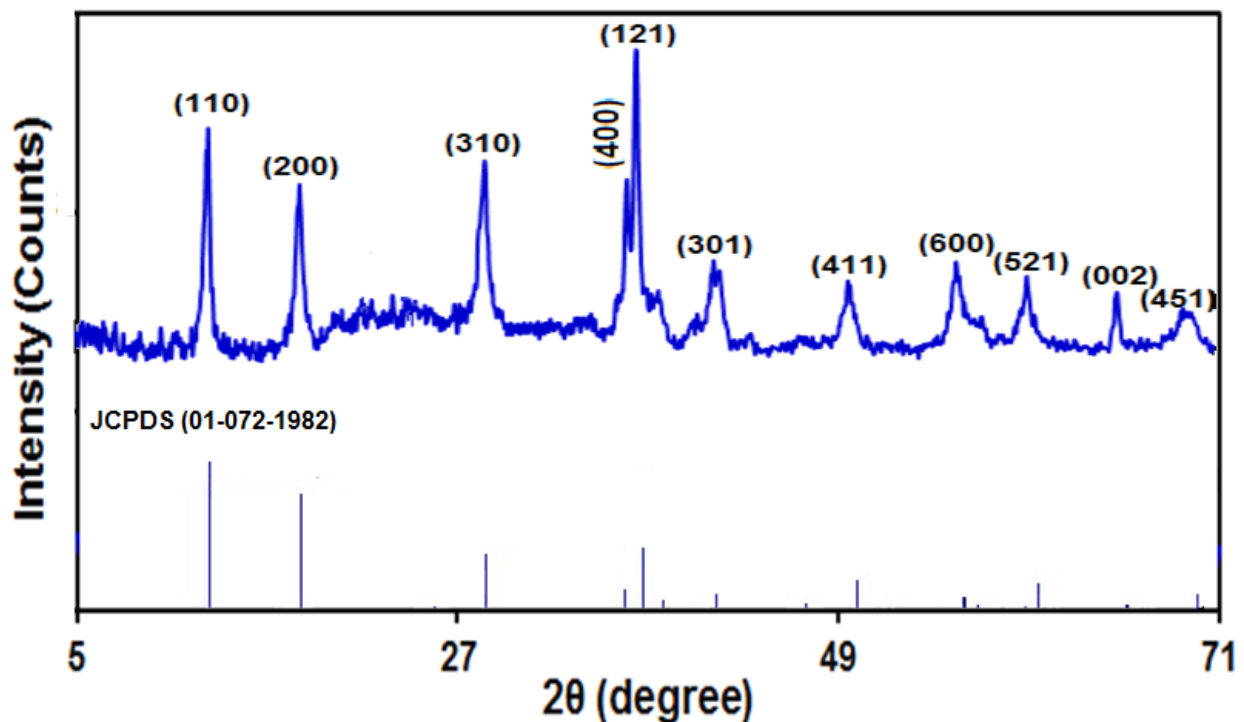


Figure 4. XRD spectrum captured for as-fabricated manganese dioxide nanorods.

3.2. Electrochemical Response of SAA on the $\text{MnO}_2\text{NR-IL/CPE}$ Surface

According to the obtained findings, the SAA electro-oxidation was based on electron and proton exchange. Moreover, it was crucial to optimize the pH value in detecting the analyte. Hence, the DPV technique was applied to clarify the electrochemical response of SAA on the $\text{MnO}_2\text{NR-IL/CPE}$ surface in PBS (0.1 M) at various pH values between 2.0 and 9.0. Reportedly, the SAA electro-oxidation on the $\text{MnO}_2\text{NR-IL/CPE}$ surface was higher in neutral conditions than in alkaline or acidic medium (Figure 5). Consequently, the optimal pH was chosen as 7.0 for SAA electro-oxidation on the $\text{MnO}_2\text{NR-IL/CPE}$ surface.

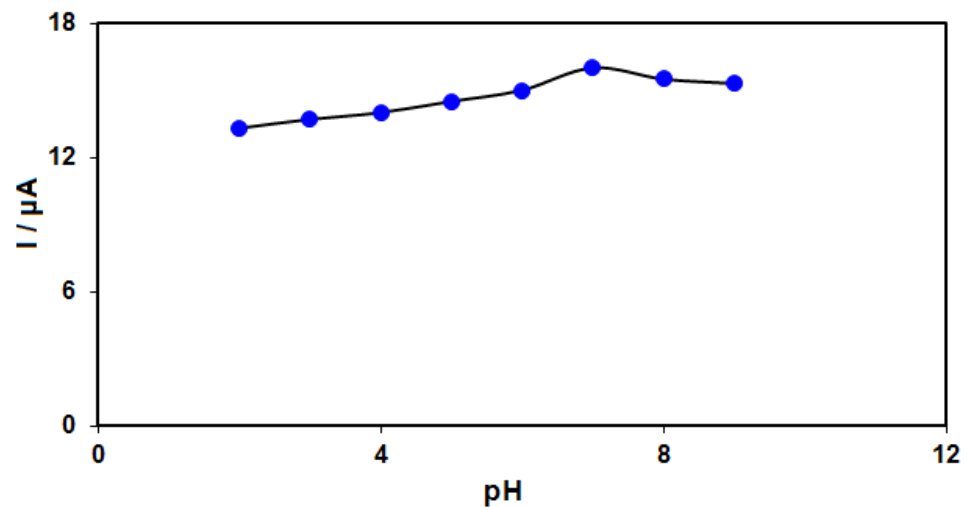


Figure 5. Plot of I_p vs. pH obtained from DPVs of $\text{MnO}_2\text{NR-IL/CPE}$ in a solution containing $50.0 \mu\text{M}$ of SAA in 0.1 PBS with different pHs (2.0, 3.0, 4.0, 5.0, 6.0, 7.0, 8.0 and 9.0).

The electrochemical performance of $\text{MnO}_2\text{NR-IL/CPE}$ in comparison with other modified electrodes was studied by the cyclic voltammetry (CV) technique under exposure to $50.0 \mu\text{M}$ of SAA at 50 mV/s in PBS (0.1 M). The CVs of all as-fabricated electrodes in this study can be observed in Figure 6. The $\text{MnO}_2\text{NR-IL/CPE}$ voltammetric behavior (Figure 6c) exhibited the relatively strongest oxidation peak at 925 mV , with the oxidation peak current at $16.0 \mu\text{A}$, sequentially. The $\text{MnO}_2\text{NR/CPE}$ voltammetric behavior (Figure 6b) exhibited the relatively strongest oxidation peak at 960 mV , with the oxidation peak current at $9.3 \mu\text{A}$, sequentially, and the bare CPE voltammetric behavior (Figure 6a) exhibited a relatively weak oxidation peak with less intensity at 1000 mV , with the oxidation peak current at $3.8 \mu\text{A}$, sequentially. Consequently, the $\text{MnO}_2\text{NR-IL/CPE}$ has an obviously better electrocatalytic behavior towards the SAA with a relatively strong current response. Additionally, bare in PBS without SAA did not show any peak.

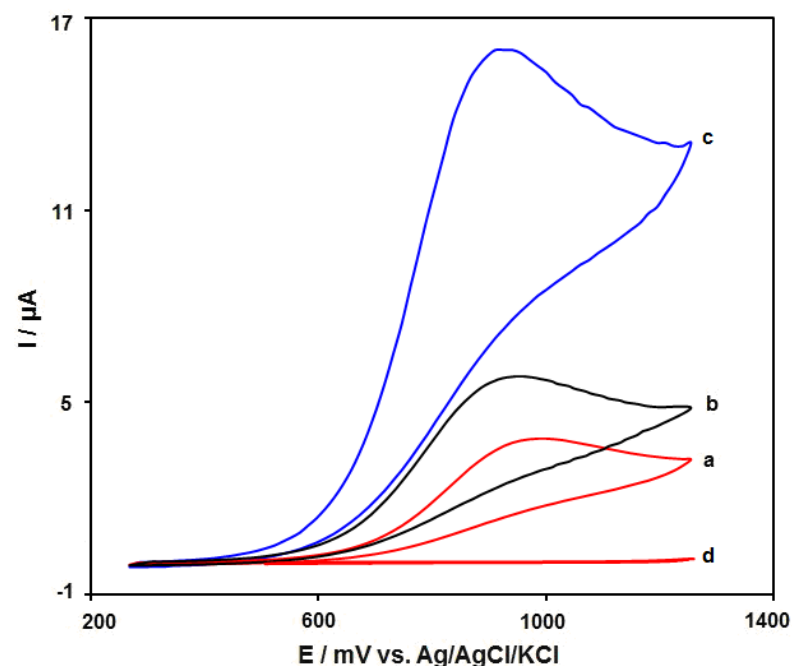


Figure 6. Cyclic voltammograms captured for (a) bare CPE, (b) $\text{MnO}_2\text{NR/CPE}$ and (c) $\text{MnO}_2\text{NR-IL/CPE}$ in PBS (0.1 M) at the optimized pH value of 7.0 under exposure to $50.0 \mu\text{M}$ of SAA at a scan rate of 50 mV/s . Additionally, (d) as (c) in the absence of SAA.

3.3. Effect of Scan Rate

The scan rate performance on the SAA oxidation peak current was investigated to analyze electrode processes. The linear sweep voltammograms (LSVs) were recorded for 50.0 μM of SAA in PBS (0.1 M) at various scan rates, and the results indicated that anodic peak currents (i_{pa}) were linearly related to the scan rate square root (Figure 7). Accordingly, the diffusion-controlled process was seen for the SAA oxidation on the $\text{MnO}_2\text{NR-IL/CPE}$.

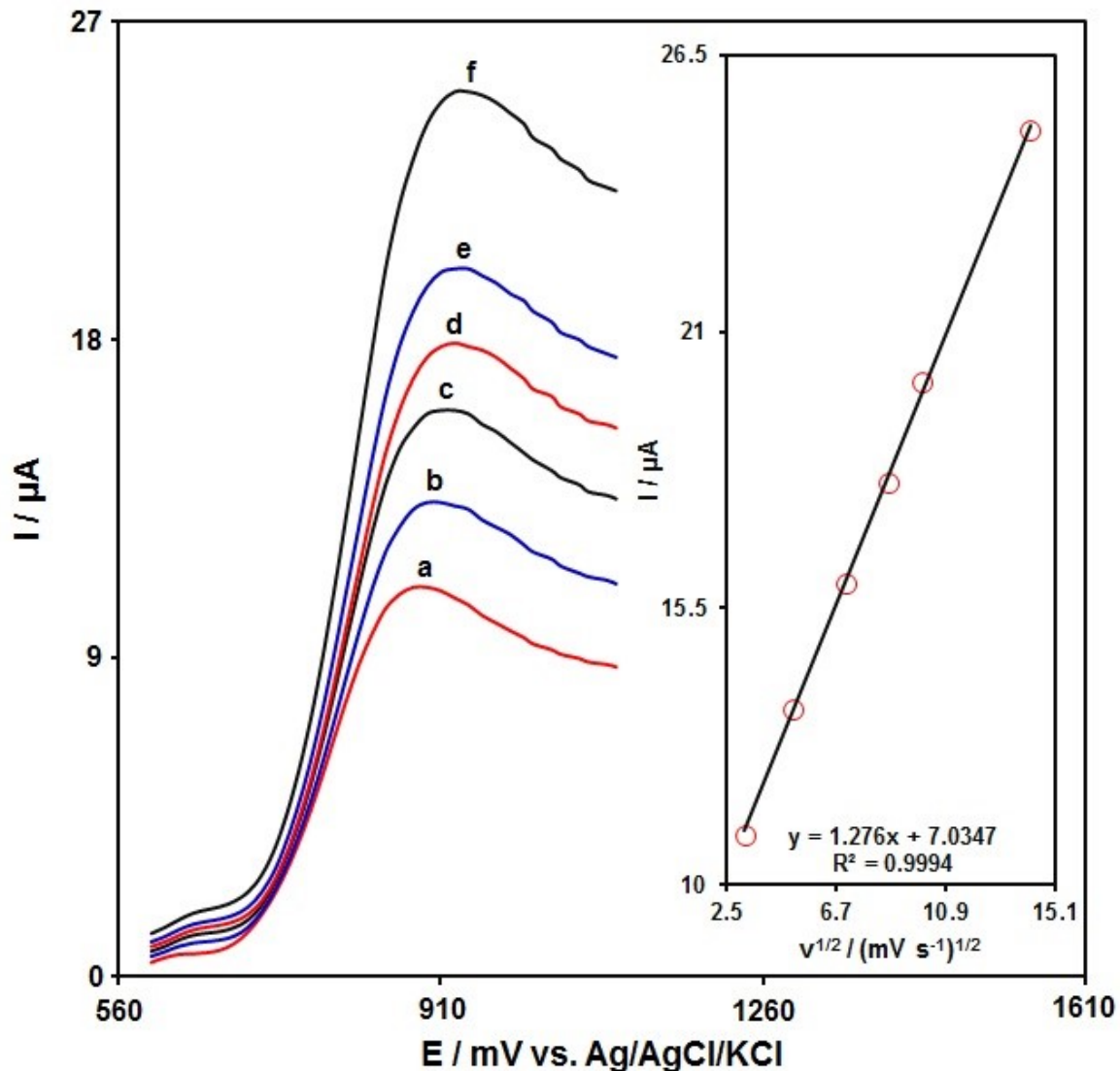


Figure 7. LSV captured for $\text{MnO}_2\text{NR-IL/CPE}$ in PBS (0.1 M) at the optimized pH value of 7.0 under exposure to 5.0 μM of SAA at various scan rates; the curves nos. a to f correspond to 10, 25, 50, 75, 100 and 200 mV/s, sequentially; Inset: changes in anodic peak currents against $v^{1/2}$.

Tafel graph was plotted to achieve data on the rate-determining step, as obtained from points of the Tafel area in linear sweep voltammetry. Figure 8 illustrates the Tafel plot for 50.0 μM SAA oxidation in PBS (0.1 M) on the $\text{MnO}_2\text{NR-IL/CPE}$ surface.

In this condition, the transfer coefficient (α) can be estimated from the slope of the Tafel plot:

$$\eta = b \log i + \text{constant}$$

where $b = 2.3RT/(1 - \alpha)nF$.

An average slope of 0.1307 V is obtained, indicating a one-electron transfer for a rate-limiting step assuming a transfer coefficient of $\alpha = 0.55$.

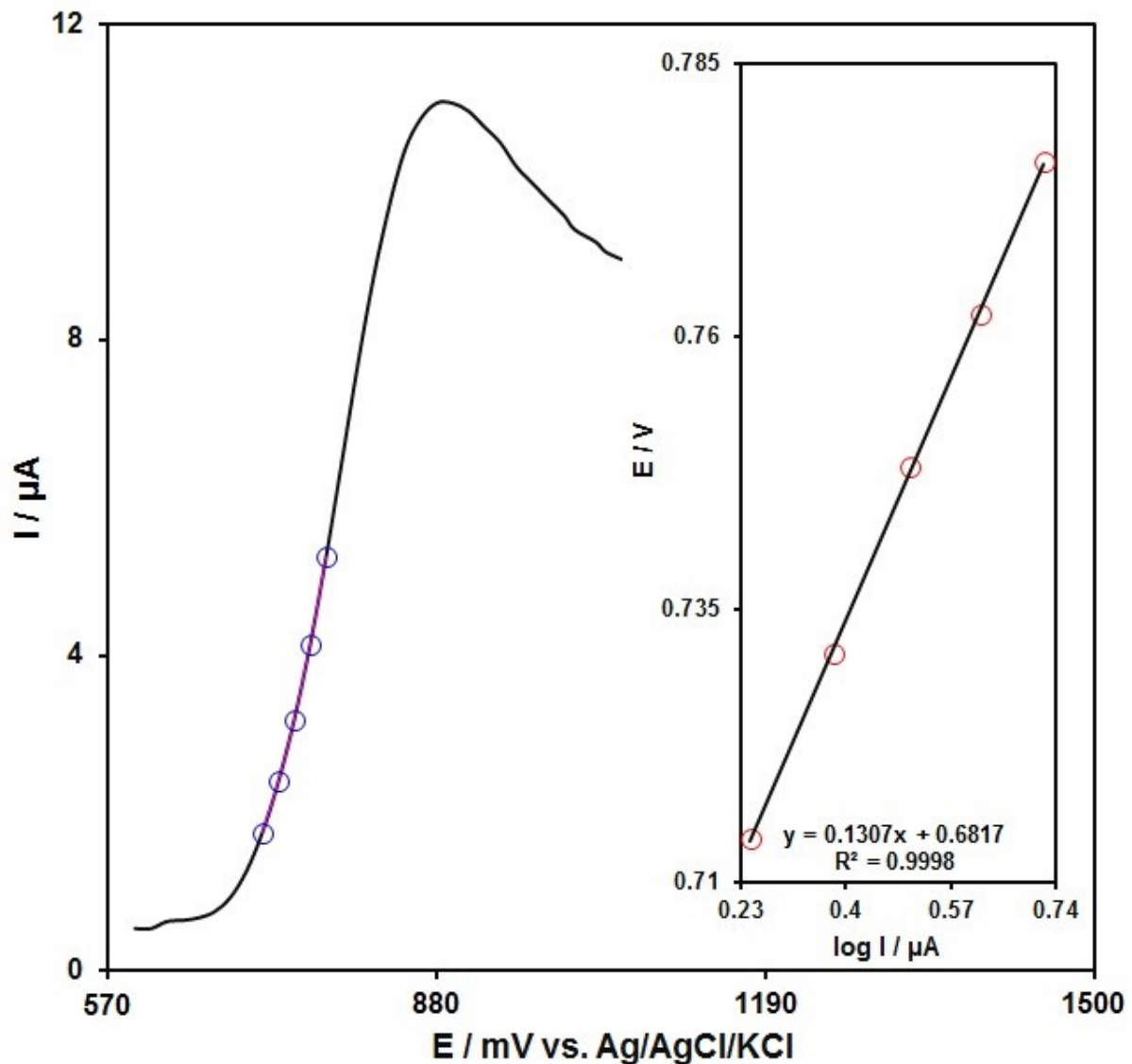


Figure 8. LSV captured for $\text{MnO}_2\text{NR-IL/CPE}$ in PBS (0.1 M) at the optimized pH value of 7.0 under exposure to $50.0 \mu\text{M}$ of SAA at 10 mV/s ; Points: information applied in the Tafel plot; Inset: LSV-derived Tafel plot.

3.4. Chronoamperometric Determinations

Figure 9 shows the chronoamperometric analysis to calculate the diffusion coefficient of SAA. The plots of I against $t^{-1/2}$ have been utilized in relation to the optimal fits for different SAA contents in PBS (0.1 M), as seen in Figure 9A. The chronoamperometric measurements were carried out for various SAA contents on $\text{MnO}_2\text{NR-IL/CPE}$ at the working electrode potential of 975 mV . The slopes of the obtained straight lines versus SAA contents were drawn by the Cottrell equation in order to obtain the below equation:

$$I = nFAD^{1/2} C_b \pi^{-1/2} t^{-1/2}$$

with D (cm^2/s) being the diffusion coefficient, n the number of electrons for oxidation of SAA ($n = 1$) and C_b (mol/cm^3) the bulk content. There was a linearity for the I against $t^{-1/2}$ plot under diffusion control over various SAA contents. The slopes could be used to compute the mean D value for SAA (see Figure 9B), which was $2.2 \times 10^{-5} \text{ cm}^2/\text{s}$.

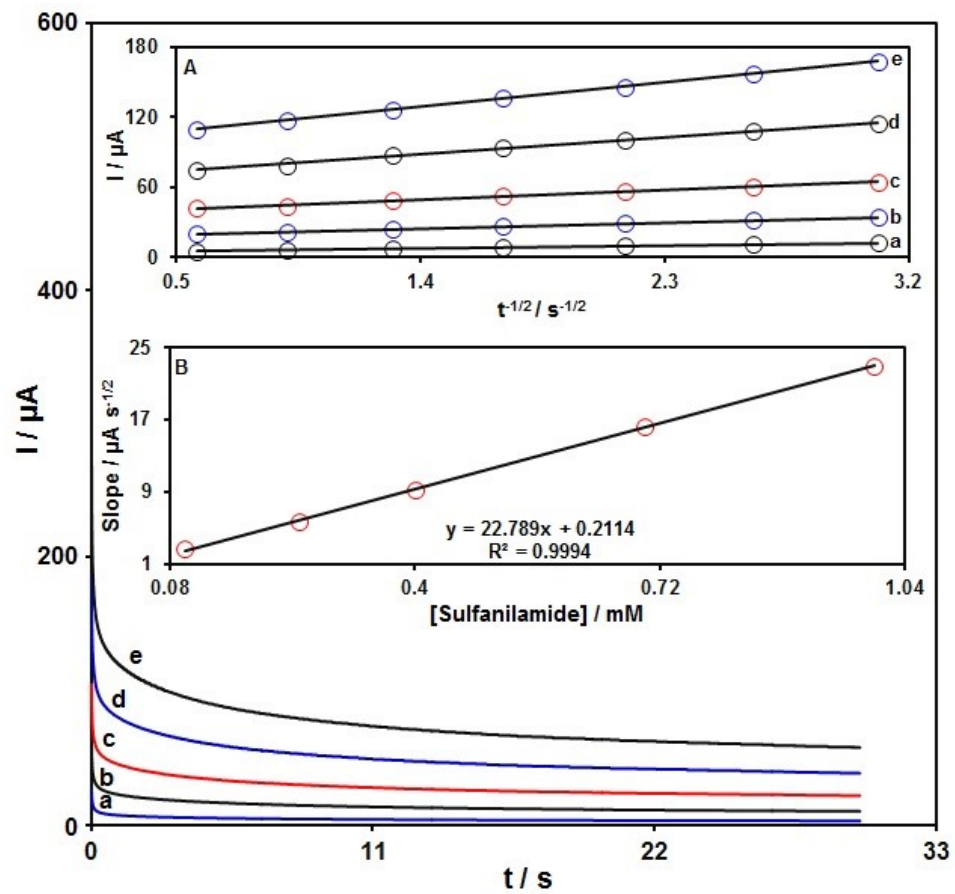


Figure 9. Chronoamperograms for MnO₂NR-IL/CPE in PBS (0.1 M) at the optimized pH 7.0 for different SAA contents; the curves nos. a to e correspond to 0.1, 0.25, 0.4, 0.7 and 1.0 mM of SAA; Insets: (A) Plots of I against $t^{-1/2}$ from chronoamperograms a to e. (B) Plot of straight lines slope against SAA content.

3.5. Detection Limit and Standard Plot

The SAA content was measured by the DPV technique. The DPVs captured for MnO₂NR-IL/CPE at various SAA contents in PBS (0.1 M) are shown in Figure 10. There was a stepwise enhancement in the SAA oxidation current by gradually increasing the SAA contents, which is to say the applicability of MnO₂NR-IL/CPE for electrochemically sensing the SAA. Figure 10 (inset) represents the alterations in the oxidation signal for MnO₂NR-IL/CPE as a function of various SAA contents (0.07–100.0 µM), showing a low detection limit of 0.01 µM. Moreover, Table 1 shows that MnO₂NR-IL/CPE can be successfully used for the determination of SAA, compared with other sensors.

Table 1. Comparison of the linear range and detection limit obtained for MnO₂NR-IL/CPE with the determination of SAA with other sensors.

Electrochemical Sensor	Method	Linear Dynamic Range	Limit of Detection	Ref.
Au nanoparticle-functionalized graphene/glassy carbon electrode	DPV	0.1–1000 µM	0.011 µM	[55]
Nanodiamond/glassy carbon electrode	Square wave voltammetry	1.2–581.4 µM	0.94 µM	[56]
Carboxylmultiwalled carbon nanotubes/glassy carbon electrode	Cyclic voltammetry	1–100 µM	0.5 µM	[57]
Fe ₃ O ₄ /functionalized Graphene/glassy carbon electrode	Amperometry	0.5–110 µM	0.05 µM	[58]
Pyrrole/molecularly imprinted polymer pencil graphite electrode	DPV	0.05–1.1 and 1.1–48 µM	0.02 µM	[59]
MnO ₂ NR-IL/CPE	DPV	0.07–100.0 µM	0.01 µM	This Work

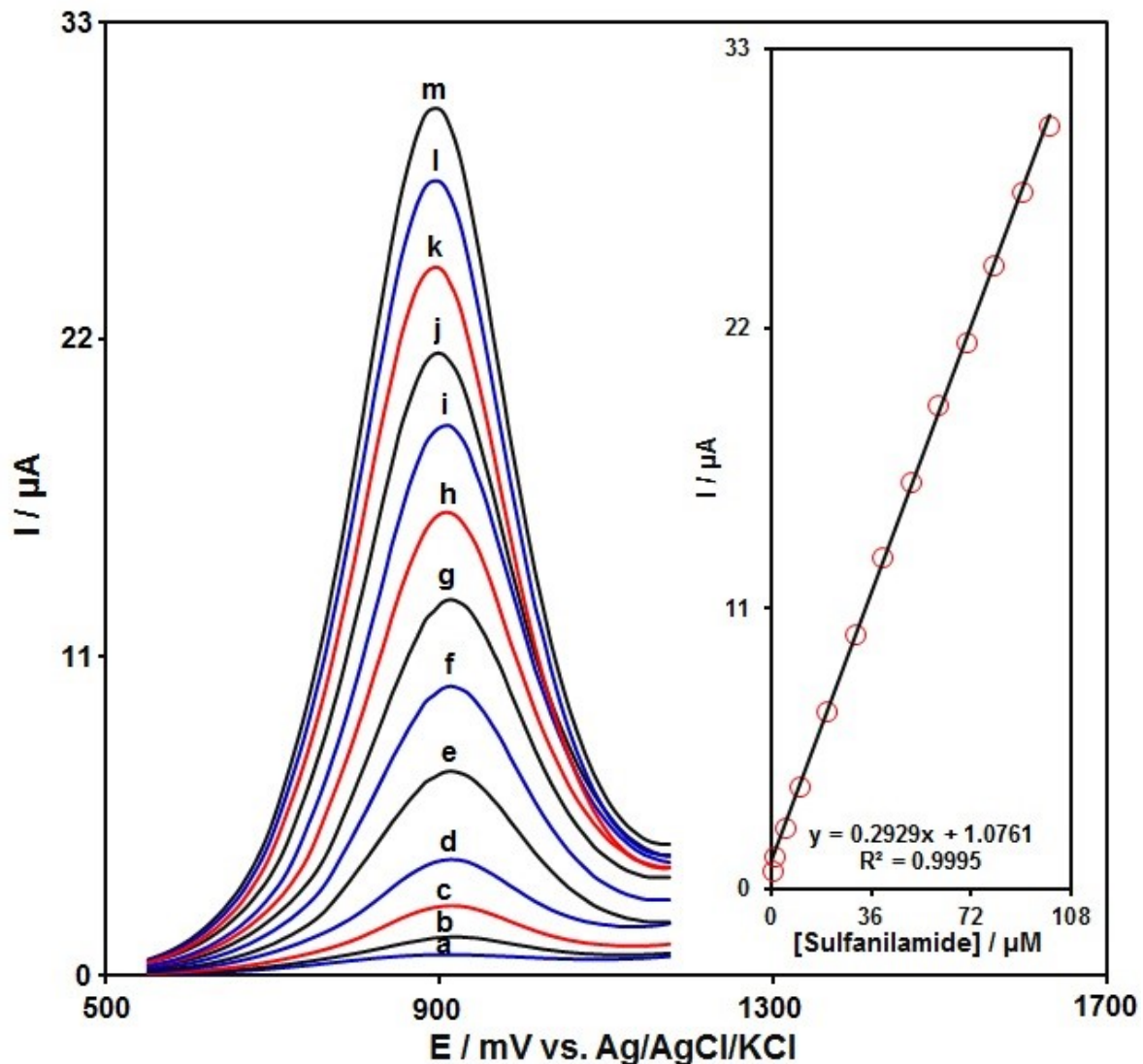


Figure 10. DPVs captured for $\text{MnO}_2\text{NR-IL/CPE}$ in PBS (0.1 M) at the optimized pH of 7.0 under exposure to various SAA contents; nos. a to m correspond to 0.07, 0.7, 5.0, 10.0, 20.0, 30.0, 40.0, 50.0, 60.0, 70.0, 80.0, 90.0 and 100.0 μM of SAA; Inset: plot of peak current as a function of various SAA contents (0.07–100.0 μM).

3.6. Interference Studies

Interference studies were investigated to know how the results for the SAA analysis were affected by the presence of various compounds. According to the used definition, the tolerance limit was defined as the ratio of the concentration of the interfering compounds to the SAA, which led to a relative error of less than $\pm 5.0\%$. The possible interference was investigated by the addition of various compounds such as Mg^{2+} , Na^+ , K^+ , Ca^{2+} , Cl^- , ascorbic acid, uric acid, glucose, sucrose, L-cystine, and dopamine to PBS (pH 7.0) in the presence of 50.0 μM SAA. It was found that the addition of these interfering species had no remarkable effect on the DPV signal of SAA. These results indicate that the modified electrode has a good selectivity for SAA determination.

3.7. Real Sample Analysis

The ability of $\text{MnO}_2\text{NR-IL/CPE}$ to be used for sensor applications in the detection of SAA was determined in real specimens of urine and water according to the standard addition method, as seen in Table 2. The recorded recovery rates ranged from 97.0% to

104.2%, thereby highlighting the appreciable applicability of MnO₂NR-IL/CPE in sensing the SAA in real specimens.

Table 2. Confirmed applicability of MnO₂NR-IL/CPE in sensing the SAA in real specimens (n = 5); all concentrations are in μM.

Sample	Spiked	Found	Recovery (%)	R.S.D. (%)
Human urine	0	-	-	-
	4.5	4.6	102.2	3.3
	6.5	6.3	97.0	2.8
	8.5	8.4	98.8	1.8
	10.5	10.6	100.9	2.3
Blood serum	0	-	-	-
	5.0	4.9	98.0	2.2
	7.0	7.3	104.3	3.5
	9.0	8.9	98.9	1.9
	11.0	11.2	101.8	2.7

4. Conclusions

A facile hydrothermal method was applied to prepare uniform and pure manganese dioxide NRs. Then, ionic liquid and MnO₂ NRs were utilized to modify a carbon paste electrode surface (MnO₂NR-IL/CPE) to voltammetrically sense the SAA. An enhanced electrochemical performance was found for the as-developed modified electrode toward SAA oxidation when compared with a bare electrode, with a lengthy linear range (0.07–100.0 μM) and a narrow limit of detection (0.01 μM). The as-fabricated sensor possessed an exceptional electrocatalytic behavior, excellent sensitivity and low limit of detection. Additionally, the MnO₂NR-IL/CPE showed a good selectivity for the detection of SAA in the presence of various compounds. The ability of the modified electrode to be used for sensor applications was verified by the determination of SAA present in actual human urine and serum specimens, with impressive recovery outcomes.

Author Contributions: Conceptualization, H.B., S.T. and A.D.B.; methodology, H.B., S.T. and A.D.B.; software, S.T.; validation, H.B.; formal analysis, S.T. and A.D.B.; investigation, S.T. and H.B.; resources, H.B.; data curation, H.B. and S.T.; writing—original draft preparation, H.B. and S.T.; writing—review and editing, S.T. and A.D.B.; visualization, S.T. and H.B.; supervision, S.T. and A.D.B.; project administration, S.T.; funding acquisition, S.T. and A.D.B. All authors have read and agreed to the published version of the manuscript.

Funding: This research was financially supported by the Research Center of Tropical and Infectious Diseases, Kerman University of Medical Sciences, Kerman, Iran (Grant Number 400000751 and research ethics committees code of IR.KMU.REC.1400.519). The APC was funded by A.D.B.

Institutional Review Board Statement: Not applicable.

Informed Consent Statement: Not applicable.

Data Availability Statement: The data presented in this study are available on request from the corresponding authors.

Conflicts of Interest: The authors declare no conflict of interest.

References

- de Moura Junior, F.G.; Veloso, W.B.; de Oliveira Junior, J.A.; Kraatz, H.B.; da Silva, I.S.; Dantas, L.M.F. Voltammetric determination of sulfanilamide using a cobalt phthalocyanine chitosan composite. *Monatsh. Chem.* **2021**, *152*, 895–902. [[CrossRef](#)]
- Wei, X.; Xu, X.; Qi, W.; Wu, Y.; Wang, L. Molecularly imprinted polymer/graphene oxide modified glassy carbon electrode for selective detection of sulfanilamide. *Prog. Nat. Sci.* **2017**, *27*, 374–379. [[CrossRef](#)]
- de Faria, L.V.; Lisboa, T.P.; Matias, T.A.; de Sousa, R.A.; Matos, M.A.C.; Munoz, R.A.A.; Matos, R.C. Use of reduced graphene oxide for sensitive determination of sulfanilamide in synthetic biological fluids and environmental samples by batch injection analysis. *J. Electroanal. Chem.* **2021**, *892*, 115298. [[CrossRef](#)]

4. Rajendiran, N.; Thulasidhasan, J. Interaction of sulfanilamide and sulfamethoxazole with bovine serum albumin and adenine: Spectroscopic and molecular docking investigations. *Spectrochim. Acta A Mol. Biomol. Spectrosc.* **2015**, *144*, 183–191. [[CrossRef](#)]
5. Lisboa, T.P.; de Faria, L.V.; Alves, G.F.; Matos, M.A.C.; Matos, R.C. Development of paper devices with conductive inks for sulfanilamide electrochemical determination in milk, synthetic urine, and environmental and pharmaceutical samples. *J. Solid State Electrochem.* **2021**, *25*, 2301–2308. [[CrossRef](#)]
6. Ferraz, B.R.; Guimarães, T.; Profeti, D.; Profeti, L.P. Electrooxidation of sulfanilamide and its voltammetric determination in pharmaceutical formulation, human urine and serum on glassy carbon electrode. *J. Pharm. Anal.* **2018**, *8*, 55–59. [[CrossRef](#)] [[PubMed](#)]
7. Dubreil-Chéneau, E.; Pirotais, Y.; Verdon, E.; Hurtaud-Pessel, D. Confirmation of 13 sulfonamides in honey by liquid chromatography–tandem mass spectrometry for monitoring plans: Validation according to European Union Decision. *J. Chromatogr. A* **2014**, *1339*, 128–136. [[CrossRef](#)]
8. Xu, S.; Wu, L. Determination of sulfacetamide sodium and sulfanilamide in shao tang ling ointment by high performance liquid chromatography. *Se Pu Chin. J. Chromatogr.* **1999**, *17*, 206–207.
9. Herrera-Herrera, A.V.; Hernández-Borges, J.; Afonso, M.M.; Palenzuela, J.A.; Rodríguez-Delgado, M.Á. Comparison between magnetic and non magnetic multi-walled carbon nanotubes-dispersive solid-phase extraction combined with ultra-high performance liquid chromatography for the determination of sulfonamide antibiotics in water samples. *Talanta* **2013**, *116*, 695–703. [[CrossRef](#)]
10. Klokova, E.V.; Dmitrienko, S.G. Spectrophotometric determination of sulfanilamides by a condensation reaction with p-dimethylaminocinnamaldehyde. *Mosc. Univ. Chem. Bull.* **2008**, *63*, 284–287. [[CrossRef](#)]
11. Wang, X.; Bryan, N.S.; MacArthur, P.H.; Rodriguez, J.; Gladwin, M.T.; Feelisch, M. Measurement of nitric oxide levels in the red cell: Validation of tri-iodide-based chemiluminescence with acid-sulfanilamide pretreatment. *J. Biol. Chem.* **2006**, *281*, 26994–27002. [[CrossRef](#)] [[PubMed](#)]
12. Santos, B.; Lista, A.; Simonet, B.M.; Ríos, A.; Valcárcel, M. Screening and analytical confirmation of sulfonamide residues in milk by capillary electrophoresis mass spectrometry. *Electrophoresis* **2005**, *26*, 1567–1575. [[CrossRef](#)] [[PubMed](#)]
13. Eren, T.; Atar, N.; Yola, M.L.; Karimi-Maleh, H. A sensitive molecularly imprinted polymer based quartz crystal microbalance nanosensor for selective determination of lovastatin in red yeast rice. *Food Chem.* **2015**, *185*, 430–436. [[CrossRef](#)] [[PubMed](#)]
14. Zargar, B.; Parham, H.; Hatamie, A. Electrochemical investigation and stripping voltammetric determination of captopril at CuO nanoparticles/multi-wall carbon nanotube nanocomposite electrode in tablet and urine samples. *Anal. Methods* **2015**, *7*, 1026–1035. [[CrossRef](#)]
15. Hatamie, A.; Echresh, A.; Zargar, B.; Nur, O.; Willander, M. Fabrication and characterization of highly-ordered Zinc Oxide nanorods on gold/glass electrode, and its application as a voltammetric sensor. *Electrochim. Acta* **2015**, *174*, 1261–1267. [[CrossRef](#)]
16. Moshirian-Farahi, S.S.; Zamani, H.A.; Abedi, M. Nano-molar level determination of isoprenaline in pharmaceutical and clinical samples: A nanostructure electroanalytical strategy. *Eurasian Chem. Commun.* **2020**, *2*, 702–711. [[CrossRef](#)]
17. Tajik, S.; Askari, M.B.; Ahmadi, S.A.; Nejad, F.G.; Dourandish, Z.; Razavi, R.; Di Bartolomeo, A. Electrochemical Sensor Based on ZnFe₂O₄/RGO Nanocomposite for Ultrasensitive Detection of Hydrazine in Real Samples. *Nanomaterials* **2022**, *12*, 491. [[CrossRef](#)]
18. Pwavodi, P.C.; Ozyurt, V.H.; Asir, S.; Ozsoz, M. Electrochemical sensor for determination of various phenolic compounds in wine samples using Fe₃O₄ nanoparticles modified carbon paste electrode. *Micromachines* **2021**, *12*, 312. [[CrossRef](#)]
19. Karimi-Maleh, H.; Khataee, A.; Karimi, F.; Baghayeri, M.; Fu, L.; Rouhi, J.; Boukherroub, R. A green and sensitive guanine-based DNA biosensor for idarubicin anticancer monitoring in biological samples: A simple and fast strategy for control of health quality in chemotherapy procedure confirmed by docking investigation. *Chemosphere* **2022**, *291*, 132928. [[CrossRef](#)]
20. Parham, H.; Rahbar, N. Square wave voltammetric determination of methyl parathion using ZrO₂-nanoparticles modified carbon paste electrode. *J. Hazard. Mater.* **2010**, *177*, 1077–1084. [[CrossRef](#)]
21. Garkani-Nejad, F.; Beitollahi, H.; Alizadeh, R. Sensitive determination of hydroxylamine on ZnO nanorods/graphene oxide nanosheets modified graphite screen printed electrode. *Anal. Bioanal. Electrochem.* **2017**, *9*, 134–144.
22. Miraki, M.; Karimi-Maleh, H.; Taher, M.A.; Cheraghi, S.; Karimi, F.; Agarwal, S.; Gupta, V.K. Voltammetric amplified platform based on ionic liquid/NiO nanocomposite for determination of benserazide and levodopa. *J. Mol. Liq.* **2019**, *278*, 672–676. [[CrossRef](#)]
23. Pushpanjali, P.A.; Manjunatha, J.G.; Hareesha, N.; D'Souza, E.S.; Charithra, M.M.; Prinit, N.S. Voltammetric analysis of antihistamine drug cetirizine and paracetamol at poly(L-Leucine) layered carbon nanotube paste electrode. *Surf. Interfaces* **2021**, *24*, 101154. [[CrossRef](#)]
24. Atta, N.F.; Galal, A.; Azab, S.M. Determination of morphine at gold nanoparticles/Nafion[®] carbon paste modified sensor electrode. *Analyst* **2011**, *136*, 4682–4691. [[CrossRef](#)] [[PubMed](#)]
25. Gholivand, M.B.; Torkashvand, M. Electrooxidation behavior of warfarin in Fe₃O₄ nanoparticles modified carbon paste electrode and its determination in real samples. *Mater. Sci. Eng. C* **2015**, *48*, 235–242. [[CrossRef](#)] [[PubMed](#)]
26. Tajik, S.; Shahsavari, M.; Sheikhshoae, I.; Garkani Nejad, F.; Beitollahi, H. Voltammetric detection of sumatriptan in the presence of naproxen using Fe₃O₄@ZIF-8 nanoparticles modified screen printed graphite electrode. *Sci. Rep.* **2021**, *11*, 24068. [[CrossRef](#)]
27. Farhadi, B.; Ebrahimi, M.; Morsali, A. Microextraction and Determination Trace Amount of Propranolol in Aqueous and Pharmaceutical Samples with Oxidized Multiwalled Carbon Nanotubes. *Chem. Methodol.* **2021**, *5*, 227–233.

28. Sanghavi, B.J.; Mobin, S.M.; Mathur, P.; Lahiri, G.K.; Srivastava, A.K. Biomimetic sensor for certain catecholamines employing copper (II) complex and silver nanoparticle modified glassy carbon paste electrode. *Biosens. Bioelectron.* **2013**, *39*, 124–132. [[CrossRef](#)]
29. Mohanraj, J.; Durgalakshmi, D.; Rakkesh, R.A.; Balakumar, S.; Rajendran, S.; Karimi-Maleh, H. Facile synthesis of paper based graphene electrodes for point of care devices: A double stranded DNA (dsDNA) biosensor. *J. Colloid Interface Sci.* **2020**, *566*, 463–472. [[CrossRef](#)]
30. Tajik, S.; Beitollahi, H.; Askari, M.B.; Di Bartolomeo, A. Screen-Printed Electrode Surface Modification with NiCo₂O₄/RGO Nanocomposite for Hydroxylamine Detection. *Nanomaterials* **2021**, *11*, 3208. [[CrossRef](#)]
31. Alavi-Tabari, S.A.; Khalilzadeh, M.A.; Karimi-Maleh, H. Simultaneous determination of doxorubicin and dasatinib as two breast anticancer drugs uses an amplified sensor with ionic liquid and ZnO nanoparticle. *J. Electroanal. Chem.* **2018**, *811*, 84–88. [[CrossRef](#)]
32. Dadamos, T.R.; Teixeira, M.F. Electrochemical sensor for sulfite determination based on a nanostructured copper-salen film modified electrode. *Electrochim. Acta* **2009**, *54*, 4552–4558. [[CrossRef](#)]
33. Saleh, T.A.; AlAqad, K.M.; Rahim, A. Electrochemical sensor for the determination of ketoconazole based on gold nanoparticles modified carbon paste electrode. *J. Mol. Liq.* **2018**, *256*, 39–48. [[CrossRef](#)]
34. Arvand, M.; Dehsaraei, M. A simple and efficient electrochemical sensor for folic acid determination in human blood plasma based on gold nanoparticles-modified carbon paste electrode. *Mater. Sci. Eng. C* **2013**, *33*, 3474–3480. [[CrossRef](#)] [[PubMed](#)]
35. Karimi-Maleh, H.; Sheikhsheoae, M.; Sheikhsheoae, I.; Ranjbar, M.; Alizadeh, J.; Maxakato, N.W.; Abbaspourrad, A. A novel electrochemical epinine sensor using amplified CuO nanoparticles and an-hexyl-3-methylimidazolium hexafluorophosphate electrode. *New J. Chem.* **2019**, *43*, 2362–2367. [[CrossRef](#)]
36. Karimi-Maleh, H.; Karimi, F.; Orooji, Y.; Mansouri, G.; Razmjou, A.; Aygun, A.; Sen, F. A new nickel-based co-crystal complex electrocatalyst amplified by NiO dope Pt nanostructure hybrid; a highly sensitive approach for determination of cysteamine in the presence of serotonin. *Sci. Rep.* **2020**, *10*, 11699.
37. Montazarolmahdi, M.; Masrounia, M.; Nezhadali, A. A New Electrochemical Approach for the Determination of Phenylhydrazine in Water and Wastewater Samples using Amplified Carbon Paste Electrode. *J. Anal. Methods Chem.* **2020**, *4*, 732–742.
38. Tajik, S.; Beitollahi, H.; Hosseinzadeh, R.; Aghaei Afshar, A.; Varma, R.S.; Jang, H.W.; Shokouhimehr, M. Electrochemical Detection of Hydrazine by Carbon Paste Electrode Modified with Ferrocene Derivatives, Ionic Liquid, and CoS₂-Carbon Nanotube Nanocomposite. *ACS Omega* **2021**, *6*, 4641–4648. [[CrossRef](#)]
39. Sanghavi, B.J.; Hirsch, G.; Karna, S.P.; Srivastava, A.K. Potentiometric stripping analysis of methyl and ethyl parathion employing carbon nanoparticles and halloysite nanoclay modified carbon paste electrode. *Anal. Chim. Acta* **2012**, *735*, 37–45. [[CrossRef](#)]
40. Mahanthappa, M.; Yellappa, S.; Kottam, N.; Vusa, C.S.R. Sensitive determination of caffeine by copper sulphide nanoparticles modified carbon paste electrode. *Sens. Actuators A Phys.* **2016**, *248*, 104–113. [[CrossRef](#)]
41. Mohammadi, S.Z.; Beitollahi, H.; Kaykhai, M.; Mohammadzadeh, N.; Tajik, S.; Hosseinzadeh, R. Simultaneous determination of droxidopa and carbidopa by carbon paste electrode functionalized with NiFe₂O₄ nanoparticle and 2-(4-ferrocenyl-[1,2,3] triazol-1-yl)-1-(naphthalen-2-yl) ethanone. *Measurement* **2020**, *155*, 1077522. [[CrossRef](#)]
42. Fekry, A.M. A new simple electrochemical Moxifloxacin Hydrochloride sensor built on carbon paste modified with silver nanoparticles. *Biosens. Bioelectron.* **2017**, *87*, 1065–1070. [[CrossRef](#)] [[PubMed](#)]
43. Karimi-Maleh, H.; Shojaei, A.F.; Tabatabaeian, K.; Karimi, F.; Shakeri, S.; Moradi, R. Simultaneous determination of 6-mercaptopruine, 6-thioguanine and dasatinib as three important anticancer drugs using nanostructure voltammetric sensor employing Pt/MWCNTs and 1-butyl-3-methylimidazolium hexafluoro phosphate. *Biosens. Bioelectron.* **2016**, *86*, 879–884. [[CrossRef](#)] [[PubMed](#)]
44. Ebrahimi, M.; Beitollahi, H. CuO nanoflowers modified glassy carbon electrode for the electrochemical determination of methionine. *Eurasian Chem. Commun.* **2021**, *3*, 19–25.
45. Ullah, N.; Ansir, R.; Muhammad, W.; Jabeen, S. Mechanistic Approaches and Current Trends in the Green Synthesis of Cobalt Oxide Nanoparticles and their Applications. *Asian J. Green Chem.* **2020**, *4*, 340–354.
46. Stanković, D.M.; Jović, M.; Ognjanović, M.; Lesch, A.; Fabián, M.; Girault, H.H.; Antić, B. Point-of-care amperometric determination of L-dopa using an inkjet-printed carbon nanotube electrode modified with dandelion-like MnO₂ microspheres. *Microchim. Acta* **2019**, *186*, 532. [[CrossRef](#)]
47. Goh, F.T.; Liu, Z.; Ge, X.; Zong, Y.; Du, G.; Hor, T.A. Ag nanoparticle-modified MnO₂ nanorods catalyst for use as an air electrode in zinc-air battery. *Electrochim. Acta* **2013**, *114*, 598–604. [[CrossRef](#)]
48. Huang, Y.; Cheng, C.; Tian, X.; Zheng, B.; Li, Y.; Yuan, H.; Choi, M.M. Low-potential amperometric detection of dopamine based on MnO₂ nanowires/chitosan modified gold electrode. *Electrochim. Acta.* **2013**, *89*, 832–839. [[CrossRef](#)]
49. Ghafour Taher, S.; Abdulkareem Omar, K.; Mohammed Faqi-Ahmed, B. Green and selective oxidation of alcohols using MnO₂ nanoparticles under solvent-free condition using microwave irradiation. *Asian J. Green Chem.* **2019**, *4*, 231–238.
50. Jaiswal, N.; Tiwari, I.; Foster, C.W.; Banks, C.E. Highly sensitive amperometric sensing of nitrite utilizing bulk-modified MnO₂ decorated Graphene oxide nanocomposite screen-printed electrodes. *Electrochim. Acta.* **2017**, *227*, 255–266. [[CrossRef](#)]
51. Prathap, M.A.; Satpati, B.; Srivastava, R. Facile preparation of polyaniline/MnO₂ nanofibers and its electrochemical application in the simultaneous determination of catechol, hydroquinone, and resorcinol. *Sens. Actuators B Chem.* **2013**, *186*, 67–77. [[CrossRef](#)]

52. Karimi-Maleh, H.; Darabi, R.; Shabani-Nooshabadi, M.; Baghayeri, M.; Karimi, F.; Rouhi, J.; Karaman, C. Determination of D&C Red 33 and Patent Blue V Azo dyes using an impressive electrochemical sensor based on carbon paste electrode modified with ZIF-8/g-C₃N₄/Co and ionic liquid in mouthwash and toothpaste as real samples. *Food Chem. Toxicol.* **2022**, *162*, 112907. [[PubMed](#)]
53. Bagheri, H.; Afkhami, A.; Shirzadmehr, A.; Khoshsafar, H. A new nano-composite modified carbon paste electrode as a high performance potentiometric sensor for nanomolar Tl (I) determination. *J. Mol. Liq.* **2014**, *197*, 52–57. [[CrossRef](#)]
54. Wang, H.; Lu, Z.; Qian, D.; Li, Y.; Zhang, W. Single-crystal α -MnO₂ nanorods: Synthesis and electrochemical properties. *Nanotechnology* **2007**, *18*, 115616. [[CrossRef](#)]
55. He, B.S.; Yan, X.H. Modifications of Au nanoparticle-functionalized graphene for sensitive detection of sulfanilamide. *Sensors* **2018**, *18*, 846. [[CrossRef](#)]
56. Li, H.; Kuang, X.; Shen, X.; Zhu, J.; Zhang, B.; Li, H. Improvement of voltammetric detection of sulfanilamide with a nanodiamond– modified glassy carbon electrode. *Int. J. Electrochem. Sci.* **2019**, *14*, 7858–7870. [[CrossRef](#)]
57. He, B.; Chen, W. Carboxyl multiwalled carbon nanotubes through ultrasonic dispersing in dimethylformamide modified electrode as a sensitive amperometric sensor for detection of sulfonamide. *Int. J. Electrochem. Sci.* **2015**, *10*, 4335–4345.
58. He, B.; Yan, S. Electrochemical determination of sulfonamide based on glassy carbon electrode modified by Fe₃O₄/functionalized graphene. *Int. J. Electrochem. Sci.* **2017**, *12*, 3001–3011. [[CrossRef](#)]
59. Tadi, K.K.; Motghare, R.V.; Ganesh, V. Electrochemical detection of sulfanilamide using pencil graphite electrode based on molecular imprinting technology. *Electroanalysis* **2014**, *26*, 2328–2336. [[CrossRef](#)]